3D global impurity transport modeling with WallDYN and EMC3-Eirene[☆]

K. Schmid[a,1,*], T. Lunt[a,]

[a] *Max-Planck-Institut für Plasmaphysik, Boltzmannstraße 2, D-85748 Garching b. München Germany*

Abstract

The global impurity migration code WallDYN was coupled to the 3D scrape off layer plasma solver EMC3-Eirene in order to make WallDYN applicable to 3D, non-toroidally symmetric, geometries. To make EMC3-Eirene suitable for migration studies its impurity transport module was extended to not just compute the impurity density in the plasma but also their deposition on the wall tiles. Originally EMC3 treats the impurity transport in the plasma as a diffusion convection problem thereby assuming immediate equilibration with the local background plasma in order to derive the local parallel convection velocity. While this is a reasonable approximation for light elements, it is not suitable for the treatment of heavy element which need significant time to equilibrate their velocity and temperature with the background plasma. Therefore EMC3-Eirene was augmented by a new kinetic impurity transport module that handles acceleration and thermalisation in a manner similar to what is implemented in the 2D trace impurity transport code DIVIMP. This paper will first describe the modification introduced in EMC3-Eirene and then show the differences between the impurity transport models and the new possibilities now available in WallDYN to interpret migration studies in non-toroidally symmetric geometries.

Keywords:

PACS: 61.80.Jh, 52.25.Vy, 52.65, 52.40.Hf

PSI Keywords: EMC3, Erosion & Deposition, Sputtering, Edge modeling

1. Introduction

The global impurity migration code WallDYN [1] has been successfully applied to interpret N accumulation studies in ASDEX Upgrade [2], model Be migration in JET and made predictions for ITER [3]. The current 2D version of WallDYN uses DIVIMP [4] for plasma impurity transport and is thus limited to toroidally symmetric geometries. While the core plasma and scrape off layer (SOL) in these devices are essentially toroidally symmetric, the details of the first wall are not: They consist of 3D structures like poloidal limiters, manipulators and gas valves, each being a toroidally asymmetric source or sink for impurities. Therefore, the calculations in e.g. [3] only gave toroidally averaged numbers of impurity deposition and layer growth. Making more detailed predictions on deposition patterns or modelling Stellerator devices such as W7-X, which are not toroidally symmetric, requires taking the 3D structure of the first wall and the far SOL into account. For WallDYN this requires switching from the 2D code DIVIMP to the 3D SOL and impurity transport code EMC3-Eirene [5]. The coupling between WallDYN and EMC3-Eirene (≡WallDYN3D) follows the same scheme as with DIVIMP: Using an EMC3-Eirene calculated background plasma, the redistribution of impurities is recorded in a charge state resolved redistribution matrix $R_{(i \to j@z)}$

[☆] Poster 193

[*] K. Schmid

Email address: klaus.schmid@ipp.mpg.de (K. Schmid)

which denotes the fraction of material launched from wall tile i that ends up on wall tile j at charge state z. The information about impurity transport in $R_{(i\to j@z)}$ is then used in WallDYN3D to calculate the redistribution of eroded material and growth of layers. The details of the basic WallDYN concept are explained in great detail in [1, 3] and will not be repeated here.

This paper will focus on the required modifications to EMC3 to make it suitable for use with WallDYN3D. Since the original EMC3-Eirene would only compute the density of the impurities in the plasma, but not the deposition of impurities on the wall tiles, a new post processing module was added that would track the impurities along field lines to the deposition location on the wall tiles. Also originally EMC3-Eirene treats impurity transport in a simplified fluid picture. It solves for the impurity density using a single diffusion convection equation with a convection velocity that is computed from the local parallel force balance. This basically amounts to an immediate acceleration of the particle to the background flow speed and thermalisation to the background plasma temperature. While this is a reasonable approximation for light elements it is not suitable for treatment of heavy element which need significant time to equilibrate their velocity and temperature with the background plasma. Therefore a new Fokker-Planck-type impurity transport module was implemented that describes the acceleration and thermalisation in a way similar what is implemented in DIVIMP. Throughout this paper we will refer to the new model as the "kinetic-" and the current model as the"diffusion convection-" model. The aim of this paper is not a general comparison of Fokker-Planck- to fluid-type impurity transport but a description of the modifications to EMC3-Eirene followed by a comparison of the current EMC3 diffusion convection with the new kinetic impurity transport model.

2. Modifications to EMC3-Eirene

The coupling of WallDYN to EMC3-Eirene was performed along the same lines as for the coupling to DIVIMP [1]: The charge state resolved redistribution matrix $R_{(i\to j@z)}$ needs to be determined for each impurity species to setup the impurity flux equation system that describes the coupling the wall elements w_i via the impurity migration in the plasma (see Eq. 3 in [1]). In addition to $R_{(i\to j@z)}$ WallDYN3D also needs the plasma temperatures $T_{e,i}$ and the main plasma species (hydrogen isotopes) ion-flux Γ_{Plasma} at each w_i, to later compute wall erosion during the WallDYN3D run. To extract $R_{(i\to j@z)}$ from EMC3-Eirene some modifications to the original EMC3-Eirene code were nescessary which will be described in the next subsections.

2.1. Impurity deposition

EMC3-Eirene uses a Monte-Carlo method for solving diffusion convection problems where the particle statistical weight can represent different physical quantities e.g. particle densities, temperatures, depending on the type of diffusion convection equation being solved. EMC3-Eirene operates iteratively [6] and advances the equilibrium solution of density & flow velocity (n_e, v_{Flow} $\rightarrow$ "Streaming iteration"), temperatures ($T_{e,i}$ $\rightarrow$ "Energy iteration"), neutrals (from Eirene) and impurity densities (n_Z $\rightarrow$ "Impurity iteration") separately in sequences, until a global equilibrium solution is reached. This makes it possible to re-use a previous plasma solution (n_e, $T_{e,i}$, v_{Flow}) to perform an impurity transport simulation (to determine $R_{(i\to j@z)}$) in trace approximation i.e. not including the feedback of the impurity radiation on the main plasma parameter, without needing to re-iterate the main plasma solution.

During the Energy and Streaming iterations the location and weight (energy $T_{e,i}$ and particle flux n_e, v_{Flow}) of each Monte-Carlo (MC) particle are stored when it's trajectory is terminated because it entered a computational grid cell

(Cell_{Final}) in contact with the wall. Based on these termination locations and weights the particle/power deposition can be calculated in a post processing step after the main plasma solution has converged. During this post processing step the MC particles are traced along field lines from Cell_{Final} onto the nearest wall tile. From the impact locations on the wall elements and the weights the power $\equiv \Gamma_{Power}$ and particle deposition $\equiv \Gamma_{Plasma}$ are computed on each wall element w_j. Similarly the $T_{e,i}$ is computed as the $T_{e,i}$ in Cell_{Final} from where the particle trace ending on w_j originated. The typical distances from Cell_{Final} along the field lines to the wall tile are of the order of the cell size (10^{-2}) m. This means in order to properly handle the plasma wall interaction the grid cells close to the wall must be small enough not just to properly sample the gradients in the plasma close to the wall, but also the variations in the first wall geometry (e.g. a poloidal limiter). Since the EMC3 plasma solution ends at the sheath entrance the small gradients and complex trajectories of particles in the sheath are not resolved in the first place. Therefore this coarse approximation is justified. More details on the sheath model are given in sub-section 3.1 where the interface between the EMC3 plasma solution and the plasma wall interaction (PWI) model in WallDYN are described

To calculate $\mathrm{R}_{(i\rightarrow j@z)}$ a single EMC3-Eirene calculation is performed for each wall element w_i whose composition evolution is to be computed later in the WallDYN3D runs. During each of these EMC3-Eirene calculations a certain flux Γ^{Src} (same for all elements and source all tiles) is emitted with an angle and energy distribution suitable for the dominate source channel (e.g. sputter erosion) of the impurity. The current version of EMC3-Eirene does not record the wall impact location of impurities, it only computes their density n_Z in each computational grid cell to later compute the radiative losses for the next Energy iteration. In order to compute $\mathrm{R}_{(i\rightarrow j@z)}$ the charge state resolved impact of the impurities needs to be extracted for each w_i. This was newly implemented into EMC3-Eirene by a scheme that is essentially identical (the new code re-uses the field line tracing routines) to the above described method for the computation of the power and particle deposition on the wall elements: During an Impurity iteration the termination cell, weight and charge state for each impurity MC particle is stored upon termination at a grid cell in contact with the wall. After the Impurity iteration, in a newly added post processing step, the impurities are traced along field lines onto the wall in a charge state resolved manner yielding the impurity flux Γ_j^{Dest} from the source w_i ending up on w_j. Finally $\mathrm{R}_{(i\rightarrow j@z)} = \Gamma_j^{Dest}/\Gamma^{Src}$ can be computed for each charge state.

In contrast to DIVIMP based 2D-WallDYN calculations the first wall in EMC3-Eirene is not closed (see also Fig. 2) but contains regions where particles can leave the computation grid without impacting on wall elements. These losses are also recorded and result in non-normalised $\mathrm{R}_{(i\rightarrow j@z)}$ which in turn results in non-closed material balance in the actual WallDYN3D calculation. In reality these losses mean that particles leave the plasma and impact on far recessed areas which are not in contact with the plasma and thus act a perfect sinks for non recycling species. Thus not affecting the correctness of the computed erosion and deposition patterns on the plasma wetted areas in the WallDYN3D calculation. However for recycling species like N these far recessed areas are not perfect sinks (unless close to a cryo-pump) and the particles may return, which needs to be taken into account in the WallDYN3D calculations. In the test calculations described in this paper we only deal with non recycling species where this difficulty does not arise. The erosion & deposition of N, where the recycling at these far recessed areas needs to be dealt with, will be the subject of a future publication.

2.2. Kinetic transport module

The Monte-Carlo (MC) based diffusion convection solver in EMC3-Eirene computes the equilibrium solution of equations like Eq. 1 where the field $F(r)$ can be n_Z, n_e, v_{Flow} or $T_{e,i}$ depending the iteration type.

$$\begin{aligned} \frac{\partial F(r)}{\partial t} &= \nabla\left(\vec{\mathbf{D}}\,\nabla F(r) + \vec{v}F(r)\right) + S(r) \qquad (1)\\ F(r) &= \text{Scalar field whose equilibrium}\\ &\quad \left(\frac{\partial F(r)}{\partial t} \equiv 0\right) \text{ value is to be calculated}\\ \vec{\mathbf{D}} &= \text{Diffusion coefficient matrix}\\ \vec{v} &= \text{Convection velocity}\\ S(r) &= \text{Sum over sources and sinks for } F(r) \end{aligned}$$

The equation is solved in magnetic field aligned coordinates by launching particles according to S(r) and updating their position parallel and perpendicular to the field based on $\vec{\mathbf{D}}$ and $\vec{v}$. The details of this position update, in particular the correct handling of curvature terms arising from the field aligned coordinates, are given in [5] but qualitatively during the impurity iteration the update during a time step $\triangle t$ occurs like in Eq. 2

$$\begin{aligned} \triangle s_\parallel &= v_\parallel \triangle t \qquad (2)\\ \triangle R, \triangle Z &= \sqrt{2\,D_\perp\,\triangle t}\\ \triangle t &= \text{Constant time step}\\ s_\parallel &= \text{Parallel position of particle}\\ \triangle R, \triangle Z &= \text{Change in perpendicular position (R, Z)}\\ v_\parallel &= \text{Local parallel convection velocity}\\ D_\perp &= \text{Local perpendicular diffusion} \end{aligned}$$

The update of $s_\parallel$ and R, Z results in a MC-trajectory of the particles through the field aligned computational grid. As the particles enter and leave grid cells, the residence time $\tau_{i,j}$ of particle j in each cell i is stored. From $\tau_{i,j}$ the equilibrium value of $F(r_i)$ in then cell located at r_i can be calculated according to Eq. 3. For instance for the computation of the impurity density n_Z particles are launched from the wall at a rate S^{Tot} in units of $\left(s^{-1}\right)$ which then from Eq. 3 yields n_Z in units of $\frac{\#}{m^{-3}}$.

$$\begin{aligned} F(r_i) &= \sum_j^n w_j\,\tau_{i,j} \qquad (3)\\ w_j &= \frac{S^{Tot}}{V_i}\\ S^{Tot} &= \text{Total source of particles}\\ V_i &= \text{Volume of cell i}\left(m^3\right) \end{aligned}$$

The current version of EMC3-Eirene treats the transport of impurities in a simplified fluid model. In contrast to the equations for the main plasma ions this fluid model for the impurities does not include separate, coupled equations for density, momentum and energy but is only comprised of a single diffusion convection equation equation as in Eq. 1 with $F(r) = n_Z(r)$. We will therefore refer to this current model simply as the "diffusion convection model". The convection velocity $v_\parallel$ is derived from a local, parallel force balance on the impurity ion in Eq. 4 (taken from [7] Eq. 6.21). $D_\perp$ is a user specified input parameter into the simulation.

$$\begin{aligned} F_\parallel &= F_{\nabla P} + F_{Fric} + F_{E_\parallel} + F_{\nabla T_e} + F_{\nabla T_i} \qquad (4)\\ F_{\nabla P} &= \text{Impurity pressure gradient force}\\ F_{Fric} &= \frac{v_{Flow} - v_\parallel}{\tau_s} = \text{Friction force}\\ \tau_s &= \text{Spitzer collision time}\\ F_{E_\parallel} &= \text{Electic force}\\ F_{\nabla T_{e,i}} &= \text{Temperature gradient forces} \end{aligned}$$

It is assumed that the impurities are in equilibrium with background plasma such that $F_\parallel \equiv 0$ is always and instantaneously fulfilled. Under these assumptions $v_\parallel$ can be computed from Eq. 4. In the absence of gradients this means that the impurity would be accelerated immediately to the background plasma flow speed thus ignoring the time required to accelerate it. While this is a reasonable choice for light impurities which due to their small

values of τ_s [8] are quickly accelerated. But for heavy ions the acceleration takes much longer thus having a large impact, in particular for long range transport. τ_s is typically in the order of 10^{-7} (sec) and at the same charge state the value for τ_s for e.g. C and W in a D background plasma differ roughly by a factor 20.

Therefore the new kinetic transport module, very similar to what is implemented in DIVIMP, was introduced in EMC3-Eirene. Due to the Monte-Carlo nature of the solver switching to the kinetic solver only requires to modify the $s_\parallel$ update in Eq. 2 by adding and update of $v_\parallel$. The perpendicular transport, the source sampling and bookkeeping routines are kept the same. In addition to $s_\parallel$, the kinetic solver updates the parallel velocity of the impurity $v_\parallel$ based on Eq. 6.33 to 6.37 and the impurity temperature T_Z based on Eq. 6.97, 6.98 taken from [7]. The update of $s_\parallel$ based on the thus computed value of $v_\parallel$ at the current time step is kept the same as in the original diffusion convection based impurity transport module. In both transport models, the impurity is initially generated as a neutral with an energy E_0 and an angle distribution appropriate for its launch type (thermal or sputtering). It is then followed along its initial velocity vector $\vec{v}_{neut}$ until it is either ionised or impacts a wall element or leaves the grid. The impurities that are ionised are then followed further as described above. The initial $v_\parallel^0$ is computed based on the local magnetic filed $\vec{B}$ as $v_\parallel^0 = \left\| \vec{v_{neut}} \cdot \vec{B} \right\|$. The initial temperature T_Z^0 is computed assuming a Maxwellian energy distribution with mean value E_0.

In addition to the update in the parallel direction the kinetic model also has different boundary conditions. The diffusion convection model uses flux boundary conditions in radial and parallel direction. In contrast the kinetic model in its current implementation simply terminates the particles when they radially leave the grid or enter a grid cell in contact with the wall. This is identical to how DIVIMP handles the termination of particles. In the future a plasma wall interaction (PWI) model will be added that would reflect & self-sputter particles given a energy and angular dependent reflection yield for the local wall material. However for the $\mathrm{R}_{(i \to j@z)}$ calculation terminating the particles is sufficient since reflection and self-sputtering is handled in WallDYN [1, 3].

3. Comparison of impurity transport models

It is instructive to compare the two transport models by computing example MC-trajectories at fixed charge states, along the parallel direction, on a constant plasma background in absence of any gradients or electrical fields. Thus only investigating the influence of the friction force and the impurity pressure gradient force. Then the diffusion convection and kinetic model reduce to Eq. 5 and Eq. 6 respectively.

$$
\begin{aligned}
\triangle s &= v_\parallel \triangle t + \sigma \sqrt{2 D_\parallel \triangle t} \qquad (5)\\
D_\parallel &= \text{Parallel diffusion Eq. 6.31 [7]}\\
v_\parallel &= v_{Flow} \text{ (in absence of gradients and } \parallel \text{ fields)}\\
\sigma &= \text{Drawn from Gaussian distribution}\\
&\quad \text{with } \langle \sigma \rangle = 1\\
&= \sqrt{-2 \log \eta_1 \cos 2\pi \eta_2}\\
\eta_{1,2} &= \text{Uniform random numbers } \in \{0, 1\}
\end{aligned}
$$

$$
\begin{aligned}
\triangle v_\parallel &= \frac{v_{Flow} - v_\parallel}{\tau_s} \triangle t + \sigma \sqrt{\frac{k_B T_Z}{m_Z} \frac{2 \triangle t}{\tau_\parallel}} \qquad (6)\\
\triangle T_Z &= \frac{T_i - T_Z}{\tau_T} \triangle t\\
\triangle s &= v_\parallel \triangle t + 0.5 \triangle v_\parallel \triangle t\\
\tau_s &= \text{Spitzer collision time (Eq. 6.35 [7])}\\
\tau_\parallel &= \text{Parallel collision time (Eq. 6.37 [7])}\\
\tau_T &= \text{Thermalization time (Eq. 6.97 [7])}
\end{aligned}
$$

The result of evaluating Eq. 5 and Eq. 6 on a reasonably chosen Deuterium background plasma with $T_e = 10$ eV, $T_i = 20$ eV, $n_e = 10^{18}$ m^{-3}, v_{Flow} = ion sound speed c_s

without evolving the impurities charge and no perpendicular transport are shown in Fig. 1. There the parallel position of C^{+2}, W^{+2} and W^{+8} as function of time step number (each $\triangle t = 10^{-8}$ s) are compared for the different transport models. Fig. 1 shows the expected result: for light impurities (large charge to mass ratio q/m), like $^{13}C^{+2}$, the difference between the kinetic and the diffusion convection picture is small, in contrast for heavy impurities with small q/m like W^{+2} the difference in the parallel position is large because of the larger τ_s it takes longer to accelerate W by the background plasma flow. However for higher charge states (e.g. +8 for W) and thus increased q/m ratio the difference reduces. This means that for light impurities the diffusion convection picture is a reasonable approximation whereas for heavy impurities the approximation is generally poorer but depends on the charge state evolution. Of course the comparison in Fig. 1 is only a qualitative measure of the influence of the new transport model. The effect on impurity deposition and main plasma impurity density can only be tested in a full EMC3-Eirene/WallDYN3D run that includes the charge state evolution as shown in the next subsection. In these calculations in addition to the friction force, also the forces due to gradients in the plasma parameters (pressure and temperatures see Eq. 4) are fully taken into account in the force calculation in both the kinetic and the diffusion convection model

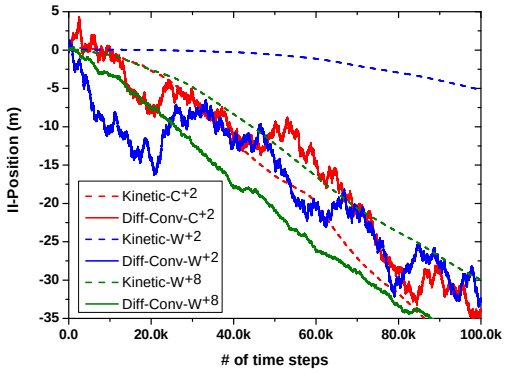

Figure 1: Comparison of example MC-trajectories for a constant background plasma and fixed impurity charge state without perpendicular transport. For small q/m ratios the difference between the kinetic and diffusion convection picture is largest whereas for large q/m ratios the difference becomes smaller.

3.1. Simulation setup

The WallDYN calculation used for testing simulates a virtual impurity seeding experiment where the impurities are introduced from the divertor dome. The simulation geometry is shown in Fig. 2. It shows the wall tiles, view rays used for diagnosing the main plasma impurity density and the seeding location. The simulation geometry encompasses 1/16-th of the ASDEX Upgrade torus and periodic boundaries are applied in toroidal direction to model the full toroidal circumference.

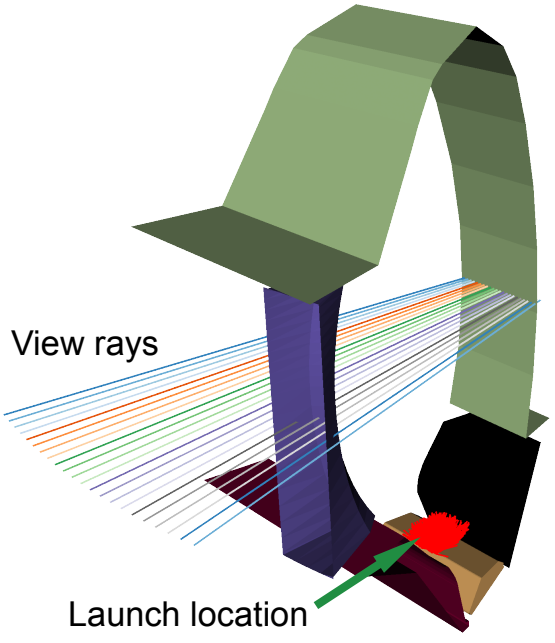

Figure 2: First wall simulation geometry including view rays for diagnosing the data on the simulation grid (not shown). Also shown is the impurity launch location at the divertor dome baffle.

In WallDYN3D the erosion, transport, deposition and re-erosion of two impurities C and W was followed. The C was seeded from the divertor dome baffle at a rate of 10^{20} (m^{-2} s^{-1}) and W originated from erosion from the full W first wall by D, C and W-self-sputtering. For simplicity it was assumed that the first wall stays at a constant temperature of 300 K in this low power L-mode plasma. The wall temperature is only of importance for the chemical re-erosion model [9] applied in WallDYN3D for any deposited C. At this low temperature chemical erosion yield is low and independent on the transport models so does not affect the model comparison. The physical sputtering and reflection yields as function of surface composition and energy are determined from SDTrim.SP [10, 11] calculations fitted with analytic models as described in detail in [1, 3]. In the SDTrim.SP calculations the impact angle of the particles (main plasma ions and impurities) due to the combination of oblique magnetic field angle and sheath ExB forces was chosen as 60° w.r.t to the surface normal following the results in [12]. The EMC3 plasma solution ends at the sheath entrance with a Bohm boundary condition (parallel velocity ≡ ion sound speed c_s) yielding T_e, T_i and Γ_{Plasma} at the sheath entrance. In a simple collisionless sheath model, the particles are therefore accelerated by the sheath potential drop of $\frac{3T_e}{e_0}$ (V) yielding and ion impact energy at charge state q of $E^q_{Ion} = 3qT_e + 2T_i$ when adding the thermal energy $2T_i$. (see [7] p. 92 Eq. 2.88). In WallDYN this is the impact energy that is used to compute sputter and reflection yields for the surface evolution model. This simple sheath model results in a plasma flux onto the surface is equal to Γ_{Plasma} thus allowing to compute erosion and reflection fluxes.

To perform this WallDYN3D calculation one $R_{(i\to j@z)}$ calculation was performed per impurity (C and W) and transport model (diffusion convection and kinetic) resulting in a total of four re-deposition matrices. They were all based on an EMC3-Eirene plasma background that was generated on a grid derived from the magnetic equilibrium of ASDEX Upgrade L-mode shot #32125. This is one of the standard test cases that a new EMC3-Eirene version has to undergo before being released to the users. It only coarsely matches the experiment and the impurity transport runs required for $R_{(i\to j@z)}$ were performed in trace approximation, using the converged equilibrium main plasma solution. In each of the wall launch EMC3-Eirene calculations 15000 test particles were launched and their charge state resolved impact location recorded as described in section 2.

In Fig. 3 the evolution of T_e and n_e at the mid-plane along the radial view lines in Fig. 2 of the background plasma used are shown. Also shown in Fig. 3 are the values of electron temperature T^{wk}_e and background plasma ion flux Γ^{wk}_D on each wall element wk partaking in the WallDYN3D calculation. Due to the 3D nature of the wall geometry it is difficult to match individual values shown in Fig. 3 to wall elements in Fig. 2. Therefore the ranges of values belonging to individual wall areas: inner & outer-target, dome, main chamber and limiter are marked by vertical lines. Thus Fig. 3 is gives only a qualitative overview of the conditions at the first wall and on the computational grid.

4. Results

In the comparison of the two transport models their influence on the impurity density in the plasma and the layer deposition rate at the first wall was investigated. To compute the impurity density for a certain gross erosion flux (sputtering + reflection + seeding) of C respectively W $\Gamma^{Gross}_{C,W}$ from the wall into the plasma the "density matrix" approach was used: For each of the EMC3-Eirene runs for the $R_{(i\to j@z)}$ calculation the charge state resolved impurity density on the computational grid $\rho^{wk,qi,ei}_{ir,ip,it}$ was stored. $\rho^{wk,qi,ei}_{ir,ip,it}$ denotes the density of element ei (C or W in this case) at charge state qi due to launch of particles with flux Γ^{Src} (same for wall wk and ei) from wall element wk at grid location. The indices ir, ip, it denote the radial-,

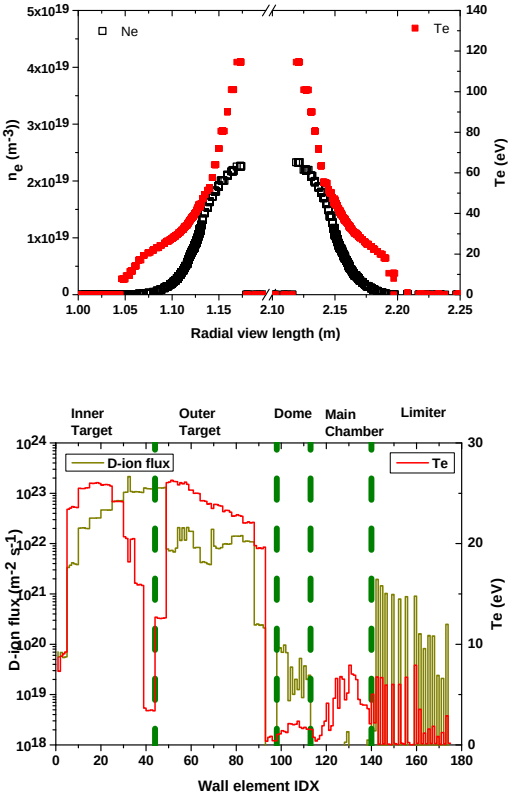

Figure 3: Electron temperature and density at the mid-plane as extracted from the view lines shown in Fig. 2. Also shown D-ion flux and electron temperature at each wall element in the WallDYN3D calculation

poloidal-, toroidal-index into the 3D computational grid. Since the calculation operates in trace approximation the impurity density for an arbitrary distribution of wall fluxes $\Gamma_{C,W}^{Gross,wk}$ from each wall element wk can be computed as a simple weighted sum as shown in Eq. 7.

$$\rho_{ir,ip,it}^{qi,ei} = \sum_{wk} \frac{\Gamma_{ei}^{Gross,wk}}{\Gamma^{Src}} \rho_{ir,ip,it}^{wk,qi,ei} \quad (7)$$

$$\rho_{ir,ip,it}^{qi,ei} = \text{Density of element ei at charge qi } (m^{-3})$$

4.1. Influence on impurity density

The impurity density was computed from $\Gamma_{C,W}^{Gross,wk}$ for the equilibrium wall state as determined by WallDYN after following the first wall composition evolution for 450 sec. The total density (sum over charge states qi) of C and W along each of the view lines shown in Fig. 2 was determined and plotted vs. position along the view line in Fig. 4.

The effect of the different transport models on the C density is benign but for W with its low q/m ration the difference is large. The reason is that due to the retarded parallel transport in the kinetic model, the distance traveled along the field, before the impurity leaves the plasma, is smaller and thus less long range transport occurs. This explains why there is less W density along the main chamber view lines. Of course this comparison relies on similar source rates for W. While C is seeded into the plasma the main source W is the erosion by the seeded C which mainly occurs in the divertor for both transport models and merely differs by $\approx 10\%$. Thus the difference in the W plasma densities can indeed be attributed to the different transport models.

4.2. Influence on layer deposition

The layer deposition rate depends not just on the rate of transport from the source to the deposition location but also on local reflection and re-erosion rates which in turn depend on the local incident flux of all impurities. This is

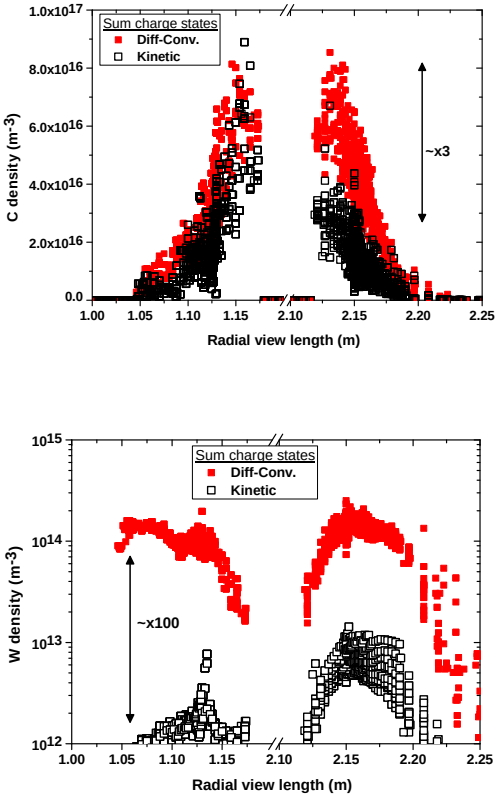

Figure 4: Difference in the total (sum over charge states) impurity density for the different transport models for C and W. While the difference for C is small the effect on W is large.

why the WallDYN concept was developed in the first place to include the process of re-erosion and re-deposition. The difference in the transport is best visualised by a plot of transport matrices for low charge states of W in Fig. 5. For the kinetic model at low q/m ratio the time needed to accelerate the particle leads to a retarded parallel transport. This means the particle has not traveled far from its source location when it leaves the plasma again resulting in more local re-deposition which manifests itself in a more diagonal re-distribution matrix.

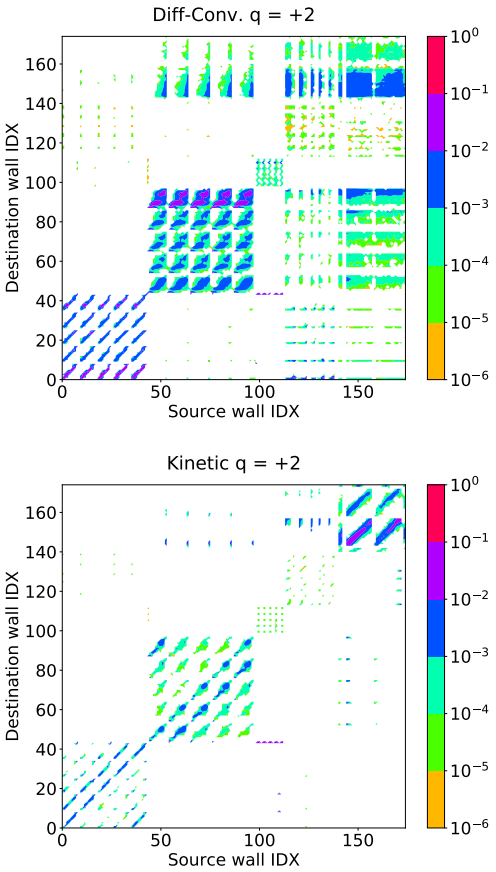

Figure 5: Redistribution matrix $R_{(i \to j@z)}$ for W computed with the standard diffusion convection and the new DIVIMP like kinetic transport model. The kinetic models retarded parallel transport leads to less long range transport and more deposition close to the origin yielding a more diagonal matrix.

This difference in the transport matrix is also reflected in the deposition rate in the main chamber region whereas the influence close to the source of both C (via seeding)

and W (via C impurity erosion) in the divertor is small: In Fig. 6 the W deposition rate for both transport models is compared. For both transport models most of the W is deposited on the inner divertor leg at similar rates but the long range transport leading to W deposition on the poloidal limiter is suppressed in the kinetic model. For C (not shown here), as before for the main chamber impurity plasma density, the difference in main chamber deposition is less pronounced.

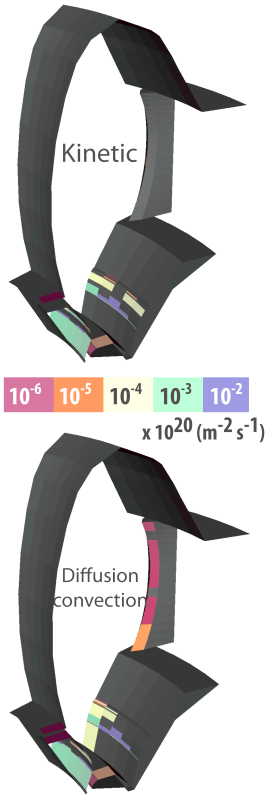

Figure 6: Net deposition region of W eroded mainly in the divertor for the different transport models. Due to the retarded long range transport there is less transport from the main impurity sources in the divertor to the main chamber and limiter in the kinetic transport model

5. Conclusions

The WallDYN model for global impurity migration and deposition was successfully coupled to the 3D SOL and impurity transport code EMC3-Eirene. This new code package WallDYN3D now allows to investigate the migration and deposition of impurities form/to non toroidally symmetric sources and sinks in Tokamaks and also handles Stellerators with their full 3D geometry. The coupling required the implementation of new routines in EMC3-Eirene to store the charge state resolved impurity deposition profiles on the first wall target elements. For better handling the transport of heavy impurities, with low charge to mass q/m ratios and therefore long acceleration and thermalisation times, a DIVIMP like kinetic impurity transport model was implemented that takes the equilibration time with the background plasma into account. A comparison of the plasma transport and WallDYN3D based impurity layer deposition rates showed that for light (large q/m) elements like C the new kinetic model is not really different from the standard diffusion convection picture. In contrast for heavy elements like W (small q/m) the differences are large. This new kinetic impurity transport model can now also be used for finding the equilibrium main plasma solutions including the influence of power loss by heavy impurity species since it can be simply turned on by a single switch in the input files. Thus it will be of use not only for migration studies but also for general SOL modelling.

[1] K. Schmid, M. Reinelt, K. Krieger, J. Nucl. Mater. 415 (2011) 284.

[2] G. Meisl, M. Oberkofler, A. Hakola, K. Krieger, K. Schmid, S. Lisgo, M. Mayer, A. Lahtinen, A. Drenik, S. Potzel, L. Aho-Mantila, A. U. Teama, the EUROfusion MST1 Team, Nuclear Materials and Energy 12 (2017) 51.

[3] K. Schmid, K. Krieger, S. W. Lisgo, G. Meisl, S. Brezinsek, J. E. Contributors, J. Nucl. Mater. 463 (2015) 66.

[4] P. Stangeby, J. D. Elder, J. Nucl. Mater. 196-198 (1992) 258.

[5] Y. Feng, F. Sardei, J. Kisslinger, P. Grigull, K. McCormick, D. Reiter, Contrib. Plasma Phys. 1-3 (2004) 57.

[6] Y. Feng, F. Sardei, J. Kisslinger, P. Grigull, J. Nucl. Mater. 241-243 (1997) 930.

[7] P. C. Stangeby, The plasma boundary of magnetic fusion devices, IOP Pulishing, 2000.

[8] L. Spitzer, Physics of fully ionized gases 2nd edn p. 120, New York: Wiley, 1962.

[9] J. Roth, C. García-Rosales, Nucl. Fusion 37 (1997) 897.

[10] W. Möller, W. E. und J. P. Biersack, Computer Physics Com-

munications 51 No. 8 (1988) 355.

[11] A. Mutzke, R. Schneider, W. Eckstein, R. Dohmen IPP-Report 12/8.

[12] K. Schmid, M. Mayer, C. Adelhelm, M. Balden, S. L. et al, Nucl. Fusion 50 (2010) 105004.